Analytical Methods

Accepted Manuscript

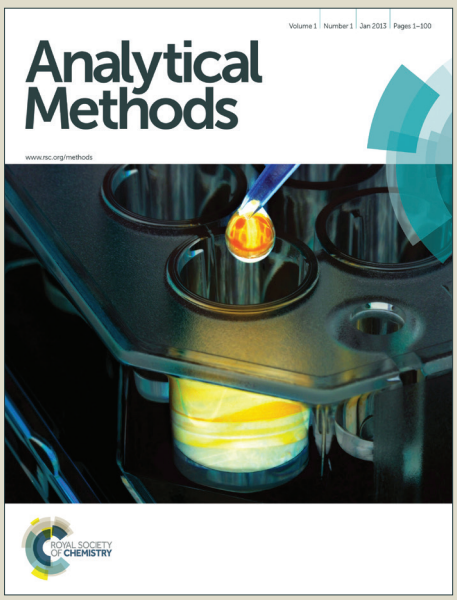

ROYAL SOCIETY OF CHEMISTRY

www.rsc.org/methods

Cite this: DOI: 10.1039/c0xx00000x

www.rsc.org/xxxxxx

ARTICLE TYPE

Electrochemical sensor based on polyaniline-modified SnO_2 nanocomposite for detecting ethephon

Zhihong Zhang[a,b*], Shuyong Zhai[b], Minghua Wang[a], Linghao He[b], Donglai Peng[b], Shunli Liu[b], Yanqin Yang[a], Shaoming Fang[a,b], Hongzhong Zhang[a,b*]

Received (in XXX, XXX) Xth XXXXXXXXX 20XX, Accepted Xth XXXXXXXXX 20XX
DOI: 10.1039/b000000x

Ethephon is a plant growth regulator and often applied in the process of the fruits growth. It could result in considerable inhibition of cholinesterase in blood plasma and erythrocytes and is very harmful to human beings once excessive consumption. The nanocomposites from polyaniline and stannic oxide (SnO_2@PANI) were synthesized and developed as the electrode material for detecting ethephon. Herein, SnO_2 nanoparticles were prepared by the method of liquid phase precipitation. Afterwards, the as-prepared SnO_2 nanoparticles were mixed with the aniline polymerization system to form the SnO_2@PANI nanocomposite. The basic chemical components of the fabricated sensor were characterized in detail using Fourier-transform infrared spectroscopy and X-ray photoelectron spectroscopy. It demonstrates that the developed SnO_2@PANI nanocomposite exhibits good electrochemical performance with relatively low charge-transfer resistance. Compared with the pristine SnO_2 and PANI, ethephon preferred to adsorb onto the SnO_2@PANI nanocomposite surface because of the synergic interaction between two components of SnO_2 and PANI. The electrochemical impedance spectra illustrated that the fabricated ethephon sensor had excellent sensitivity, with a detection limit of 4.76 pg mL^{-1} within the range from 0.01 to 5 ng mL^{-1}. Moreover, the developed electrochemical biosensor exhibits good selectivity and stability. All of these food performances provide a promising tool to detect the illegal food additives.

Introduction

Ethephon [2-chloroethylphosphonic acid] is a plant growth regulator that is normally used to promote pre-harvest ripening of several vegetable products, facilitate the harvest of fruit, and accelerate post-harvest ripening [1]. This compound has several uses including straw shortening and strengthening to increase resistance to lodging (cereals), promotion or inhibition of flowering (fruit trees, pineapples, and ornamental plants), promotion of maturation and coloring (tomatoes, sweet peppers, apples, pineapples, and wine grapes), enhancement of sugar content (sugar cane), induction of fruit abscission (cherries), or uniform boll opening (cotton) to facilitate harvest. However, ethephon results in considerable inhibition of cholinesterase in blood plasma and erythrocytes in long-term feeding tests on dogs and rats. Harmful accumulation of this inhibitor in food can be prevented by appropriate applications based on residue analysis [2].

[a] *Henan Collaborative Innovation Center of Environmental Pollution Control and Ecological Resoration,*
[b] *Henan Provincial Key Laboratory of Surface and Interface Science, Zhengzhou University of Light Industry, No. 166, Science Avenue, Zhengzhou 450001, P. R. China E-mail addresses: mainzhh@163.com or zhz@zzuli.edu.cn;Tel:+008686609676*

*

The phosphonic acid group in ethephon provides the high polarity, water solubility, and low volatility of the molecule [3, 4]. These properties make it difficult to directly determine, either by liquid chromatography- or gas chromatography-based methods. Moreover, ethephon decomposes easily to ethylene at pH >4, at high temperature, or under UV radiation due to its low stability. Thus, ethephon has been indirectly determined by measuring the quantity of ethylene released after increasing either pH or temperature [5, 6], with limits of detection (LOD) between 0.02 mg/kg-0.1 mg/kg. Liquid chromatography [7], chemiluminescence [8], spectrophotometry [9], mass spectrometry [10], and fluorescence [11] have been used for detecting ethephon. However, these methods are tedious, time consuming, complex, and expensive. Electrochemical methods are the most promising techniques for detecting various analytes because of their simplicity, high reliability, high sensitivity, high selectivity, low cost, fast response, and ease of use [12-14].

As known, nanostructural metal oxide semiconductors possess high surface area, good biocompatibility, catalytic activity, and chemical stability. Among the metal oxide semiconductors, SnO_2, a p-type semiconductor with a wide bad gap of 3.6 eV at 300 K, has been investigated for various applications such as in solar cells, electrochemical sensors, and

biosensors [15-17]. Meanwhile, polyaniline is a unique conducting polymer because of its chemical and environmental stability, facile synthetic method, and readily controlled doping dopants [18-20]. SnO_2 and PANI are often used as sensitive layers for DNA biosensor [17, 21]. Numerous reports have been published on the fundamental performances and its applications of high-performance supercapacitors and biosensors of SnO_2@PANI nanocomposites [22-26]. For example, introduction of a small quantity of SnO_2 and its intercalation in the polymer matrix significantly influences the surface morphology, optical properties, electrical conductivity, thermal stability, and electrochemical properties of prepared nanocomposites [27-31]. The electrical conductivity of SnO_2@PANI nanocomposite is highly desirable than pure PANI [27]. Therefore, investigating the electrochemical properties of SnO_2@PANI composites is more valuable for the superconductor electrode applications compared with the previous report.

Given the immobilization of DNA strands onto biosensors based on PANI or SnO_2 films [17, 21], ethephon could be adsorbed onto the surface of these nanomaterials because of the same functional phosphate groups in DNA and ethephon. Thus, this study was designed to demonstrate the possibility of ethephon adsorption onto the SnO_2@PANI nanocomposites, showing the potential of such composite-based electrochemical biosensors for detecting ethephon. Compared with the routine methods, the prepared electrochemical biosensor based on the SnO_2@PANI nanocomposites shows two advantages. The first is the large amount of amino groups of PANI within the composites to further improve the affinity of the small molecules containing rich phosphate groups. The other advantage is that the possible synergistic effect between SnO_2 and PANI provides the improvement for anchoring ethephon, leading to an extremely low detection limitation of 4.76 pg mL^{-1} toward ethephon.

Experimental Sections

Materials

Aniline (purchased from Tianjin Kermel Chemical Reagent Co., Ltd., analytical purity) was distilled under reduced pressure before use. NaOH, HCl (37 %), $SnCl_4 \cdot 5H_2O$, and $(NH_4)_2S_2O_8$ (purchased from Sinopharm Chemical Reagent Co., Ltd.) were all of analytical grade and used as received. All solutions were prepared with Milli-Q water (≥18.2 MΩ·cm^{-1}). All other chemicals, including anhydrous ethanol, methyl alcohol, hydrogen peroxide, and petroleum ether, were used as received.

Preparations

Preparation of SnO_2 nanoparticles. SnO_2 nanoparticles (SnO_2 NPs) were prepared by the method of liquid phase direct precipitation [32]. In a typical experiment, 2.4 g NaOH (0.06 mol) was dispersed in 40 mL of Milli-Q water to form a clear solution. 3.5 g $SnCl_4 \cdot 5H_2O$ (0.01 mol) was then added under vigorous stirring. Simultaneously, 20 mL of anhydrous ethanol was added to the solution dropwise. After stirring for 10 min, the solution was transferred to the reaction and maintained at 210 °C for 24 h. After the system cooled down, the white precipitate was removed and washed for five times with anhydrous ethanol. Finally, the precipitate was transferred to the vacuum drying oven and dried at 60 °C for 18 h.

Synthesis of SnO_2@PANI nanocomposites. 0.15 g SnO_2 was added into HCl (1.5 mol/L) to form the homogenous solution, followed by being ultrasonically oscillated for 0.5 h. Afterwards, the solution was transferred to a flask and was put into the ice-water bath with stirring intensely. Moreover, aniline was added into the SnO_2 solution and stirred continuously for 0.5 h. $(NH_4)_2S_2O_8$ {n [$(NH_4)_2S_2O_8$]: n (aniline) =1:1} was dissolved into 20 mL HCl (1.5 mol/L) and dropped slowly into the mixture of aniline and SnO_2. The solution was then stirred in ice-water bath for 3.5 h. The color of the solution changed from oyster white to dark green, indicating the production of polyaniline. The resultant solution was filtered and washed successively with HCl and deionized water until no white precipitate could be created with $BaCl_2$ (0.1 mol/L). Successively, the solution was washed with acetone until the solution color was unchanged. Finally, the dark green filter cake was dried in the vacuum oven under 60 °C for 24 h. The viridis SnO_2@PANI nanocomposite was obtained.

The process of the composite electrodes modified with PANI, SnO_2 NPs, and SnO_2@PANI nanocomposites. 0.5 mg SnO_2@PANI nanocomposite was added to Millin-Q water and being ultrasonic thoroughly until a homogeneous suspension of SnO_2@PANI was obtained. Similarly, 0.5 mg mL^{-1} SnO_2 NPs and 0.5 mg mL^{-1} PANI homogeneous suspension was obtained. The as-prepared suspension of SnO_2 NPs, PANI, and SnO_2@PANI nanocomposite was stored under refrigeration at 4 ℃ for further use.

Au electrodes (3 mm diameter) were polished with 0.05 μm alumina slurries, ultrasonically washed in Millin-Q water and electrochemically cleaned through a series of oxidation and reduction cycling in 1.0 M H_2SO_4 from -0.4 V to 1.2 V (vs Ag/AgCl). The Au electrodes modified with SnO_2@PANI were prepared by dropping 5 μL of the corresponding suspension (0.5 mg mL^{-1}) onto the Au electrodes and being dried at room temperature. The similar modification procedure was used to prepare the composite electrodes composited with PANI and SnO_2 NPs.

Preparation of phosphate buffer, electrolyte and ethephon solutions. Phosphate buffer solution (PBS) was prepared by mixing 0.067 M Na_2HPO_4 and 0.067 M KH_2PO_4 in an 8:2 ratio of $v(Na_2HPO_4)$:$v(KH_2PO_4)$. Electrochemical measurements was recorded in solution of 8 g of NaCl and 0.2 g of KCl and 1.65 g of $K_3[Fe(CN)_6]$ and 2.11 g of $K_4[Fe(CN)_6]$. A stock solution of 1 mg mL^{-1} ethephon standard was prepared by dissolving 10 mg ethephon powder in 10 mL of Millin-Q water. Afterwards, it was stored in the dark at -20□. Working ethephon solution was prepared by diluting the stock solution in Millin-Q water to obtain the concentrations of 0.01, 0.1, 0.5, 1, and 5 ng mL^{-1}.

Preparation of real samples. The orange, apple and strawberry juice samples were obtained from local market (Zhengzhou, China). Fruit juice samples were stored in the specific food containers at 4 ◦C and analyzed within 3 days. A 25 mL aliquot of fresh juice was centrifuged at 3500 rpm for 15 min, and then the supernatant was filtered through a 0.22 μm membrane filter into

50 mL conical flask. Before extraction, 25 mL of filtrate was diluted at 1:1 ratio with PBS in a volumetric flask of 50 mL. The water sample (lake water) was filtered through a 0.22 μm membrane and the pH was adjusted to 7.4.

Characterization studies

The chemical structure and components were analyzed by X-ray photoelectron spectroscopy (XPS) using a VG ESCALAB HP photoelectron spectrometer equipped with an analyzer and preparation chambers. Fourier-transform infrared (FTIR) spectra were recorded on a Bruker TENSOR27 spectrometer (32 scans at a resolution of 4 cm^{-1}). The crystal structure of the SnO_2@PANI hybrid material was examined by XRD (D8 Advance diffractometer with Cu Kα radiation at 40 kV and 100 mA). Surface morphology was analyzed with SEM (JSM-6490LV, Japan, operated at 25 kV).

Electrochemical measurements

Electrochemical impedance spectroscopy (EIS) was performed using a CHI660D electrochemical analyzer (Shanghai Chenhua, China). A conventional three-electrode cell was used, which included an Ag/AgCl (saturated KCl) electrode as reference electrode, platinum slides as counter electrodes, and the Au electrode modified wit the pristine SnO_2 nanoparticles, PANI, and SnO_2@PANI nanocomposites as working electrodes.

Data of electrochemical impedance spectroscopy (EIS) were collected at a potential of 0.2 V in the frequency range of 1 mHz to 1 MHz, with an alternating current amplitude of 5 mV. The EIS spectra were analyzed using Zview2 software, which uses a nonlinear least-square fit to determine the parameters of the elements in the equivalent circuit. All electrochemical experiments were carried out at room temperature (25 ± 1 ℃).

Results and discussion

Chemical composition and crystal structure of SnO_2 and SnO_2@PANI

Fig. 1a shows the results of powder XRD pattern of the as-prepared SnO_2 and resultant SnO_2@PANI nanocomposite. The XRD spectroscopy of the pristine SnO_2 nanoparticles indicates that SnO_2 is well-crystallized and reveals all diffraction peaks, which are perfectly similar to the JCPDS data (Card No. 41-1445) (cave i). The XRD pattern of the SnO_2@PANI nanocomposites indicates that the nano-SnO_2 is also present in the composites (cave ii). The diffraction patterns of the SnO_2@PANI nanocomposites are similar to that of nano-SnO_2, indicating that PANI did not affect the crystallization performance of nano-SnO_2. No apparent peak was observed in the XRD spectrum of PANI since PANI is amorphous (cave ii).

Fig. 1b shows the FTIR spectra of the as-prepared SnO_2. PANI, and SnO_2@PANI. The broad adsorption band centered at 617 cm^{-1} is attributed to the oxide-bridge functional group (νO Sn-O) [33]. The PANI obtains the IR bands at ~1562 cm^{-1} and ~1477 cm^{-1}, corresponding to the stretching vibration of C=N and C-C in benzenoid or quinonoid rings, respectively [34, 35]. The peaks at 1299 cm^{-1} and 1242 cm^{-1} are attributed to the stretching vibrations of C-N in benzenoid rings [36]. The strong peak at 1136 cm^{-1} is due to the in-plane bending vibration of benzenoid or quinoid C-H [34, 35, 37]. The bands around 879-705 cm^{-1} correspond to the out-of-plane bending vibrations of benzenoid or quinonoid C-H and N-H [37, 38]. In the FTIR spectrum of SnO_2@PANI, Sn-O-Sn symmetric stretching, which should occur in the range of 500--750 cm^{-1}, was observed. In addition, the peaks of SnO_2@PANI exhibits all other absorption bands compared with the characteristic absorption bands in PANI.

XPS analysis was performed to verify the chemical compositions before and after the detection of ethephon using the developed electrochemical biosensor. The atomic % of the samples is presented in Table S1. It demonstrates that there are four elements, i.e., C 1s, Sn 2d, N 1s, and O 1s, in the SnO_2@PANI nanocomposites. After the ethephon adsorption, 8.21% P 2p and 1.05% Cl 2p were observed, indicating the presence of ethephon in SnO_2@PANI nanocomposites. The XPS core-level spectra of C 1s, N 1s, Sn 2d, O 1s, P 2p, and Cl 2p of the samples are summarized in Fig. 2. As for C 1s core-level XPS spectrum of SnO_2@PANI nanocomposites (Fig. 2a), it was fitted into three peaks. The peak at ~284.6 eV is assigned to C-C/C-H, which was very slight in the FTIR spectrum of SnO_2@PANI nanocomposites. The peak at ~285.1 eV is due to C=C, whereas the peak at ~285.7 eV is possibly attributed to C-N. ~286.6 eV was appeared, which could be due to C-Cl (Fig. 2c) [39, 40], which was resulted from ethephon. The N 1s core-level XPS spectrum of SnO_2@PANI nanocomposites only contains one main peak at

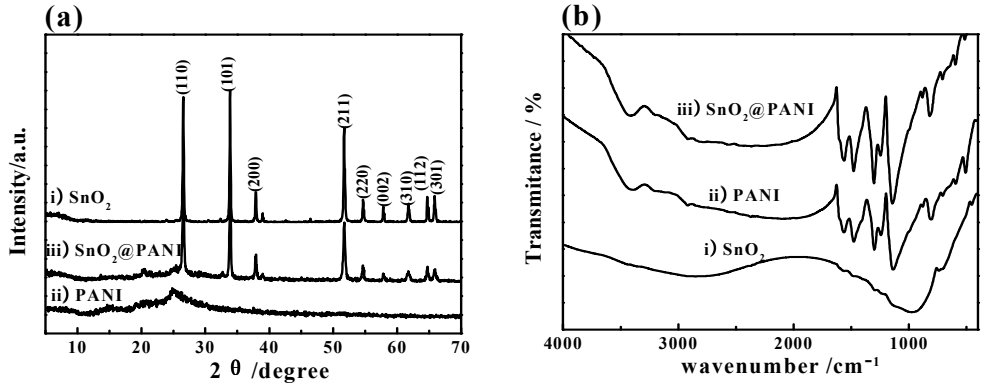

Fig. 1 (a) XRD and (b) FTIR spectra of the as-prepared SnO_2, and SnO_2@PANI nanocomposites.

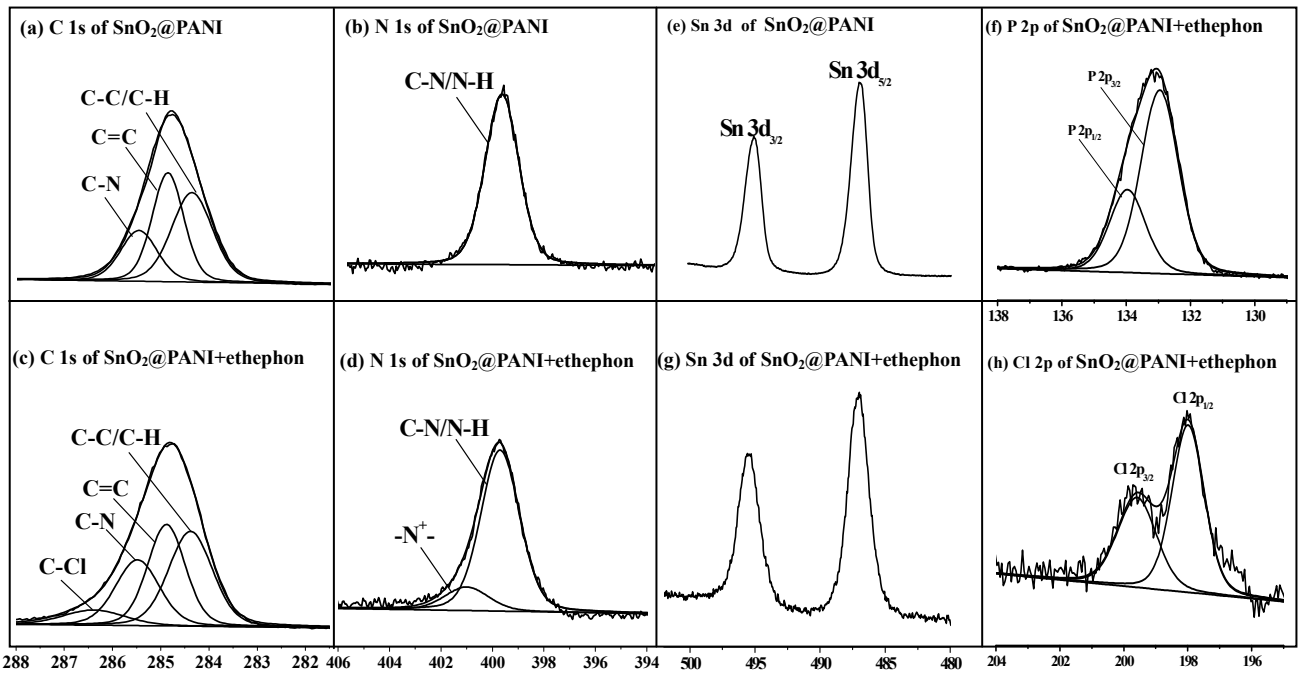

Fig. 2 (a) C 1s, (b) N 1s, (c) Sn 2p and (d) O 1s core-level XPS spectra of SnO_2@PANI and (e) C 1s, (f) N 1s, (g) Sn 2d , (h) O 1s, (i) P 2p and (j) Cl 2p core-level XPS spectra of SnO_2@PANI adsorbed with ethephon.

~399.4 eV, indicting the presence of C-N and N-H groups (Fig. 2b). When ethephon was adsorbed onto the SnO_2@PANI surface in the aqueous solution, a new peak at ~401 eV in N 1s core-level XPS spectrum was observed and due to the $-N^+-$ groups, which could be resulted from the protonation of $-NH_2$ of PANI in aqueous solution (Fig, 2d) [41]. As shown in Fig. 2e and g, substantial Sn 2d signals were observed in the core-level XPS spectrum in two samples, in which the two separated peaks at ~487.2 and ~495.6 eV are assigned to Sn $2d_{5/2}$ and Sn $2d_{3/2}$, respectively [42]. In addition, two peaks were separated out at ~133 and ~134 eV in the XPS core-level spectrum of P 2p, which are mainly due to P $2p_{3/2}$ and P $2p_{1/2}$ (Fig. 2f) [43]. Moreover, it is clear that Cl 2p spectrum can be curve-fitted with two peaks components with binding energies at ~200 and ~201.6 eV, which are associated with Cl $2p_{3/2}$ and Cl $2p_{1/2}$ (Fig. 2h), respectively [39, 44]. All of these results showed that ethephon was successfully adsorbed on the SnO_2@PANI surface.

Surface morphology of the samples

SEM micrographs of SnO_2, PANI, and SnO_2@PANI nanocomposites were summarized in Fig. 3. SnO_2 has submicron-sized/ nanosized spherical grains with a few agglomerations (Fig. 3a). Elongated PANI nanowires were observed and piled together loosely (Fig. 3b). In Fig. 3c, the SEM micrographs show that the nanostructured SnO_2 particles are apparently embedded within the PANI chains. According to the BET analysis, the specific surface area of the composite material was obtained as 14.332 $m^2 g^{-1}$ (Fig. S2). This finding implies that the composite is highly aggregated and could not strongly adsorb ethephon only through the physical interaction.

Detection of ethephon using the developed electrochemical sensor based on SnO_2, PANI, and SnO_2@PANI nanocomposite

EIS is an effective tool to monitor changes in the surface features of modified electrodes during the assembly process. This technique was used in the DNA electrochemical biosensor [45], proteins [46], or binding behavior of other biomolecules [47]. The

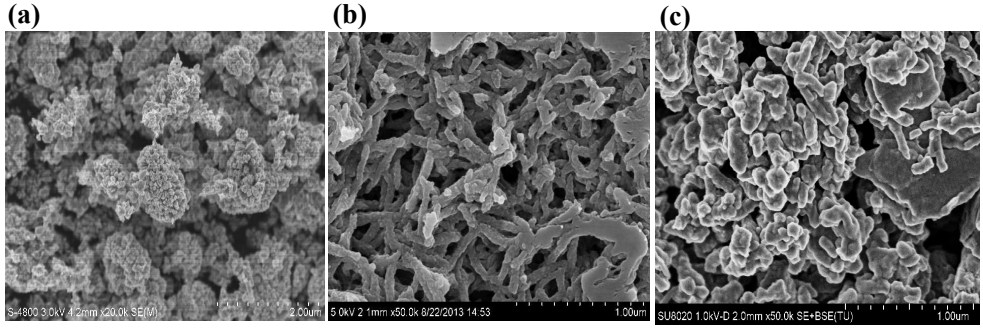

Fig. 3 SEM micrographs of (a) SnO_2, (b) PANI, and (c) SnO_2@PANI nanocomposite.

impedance spectrum includes a semicircle and a linear portion (Fig. S1). The semicircle portion at high frequencies corresponds to the electron transfer process, whereas the linear portion at lower frequencies represents the diffusion process. The semicircle diameter is equal to the electron-transfer resistance R_{ct} [48]. Fig. 4 shows the EIS of the electrode at various stages for ethephon detection based on SnO_2, PANI, and SnO_2@PANI nanocomposite. The impedance data were fitted to a Randle modified equivalent circuit [28], as shown in Fig. 4a (inset), that includes the electrolyte resistance between working and reference electrodes (R_s), Warburg impedance (Z_w), resulting from the diffusion of ions to the interface from the bulk of the electrolyte, electron-transfer resistance (R_{ct}), and electrode/electrolyte interface capacitance (C) (Fig. S1). The bare Au electrode showed the lowest charge transfer resistance (R_{ct}) value. It demonstrates that the experimental impedance data (dot) are consistent with a fitted data (line) with Zview2 software, (CHI 660). Charge-transfer resistance, R_{CT}, is the result of resistance to charge transfer from the $[Fe(CN)_6]^{3+/4+}$ redox probe to the electrode surface through the composite electrode. In case of the ethephon adsorption on the pristine SnO_2 nanoparticles (Fig. 4a), the bare gold electrode exhibits an almost straight line, and its R_{ct} is 0.12 kohm. When SnO_2 nanoparticels were coated onto the bare gold electrode, the R_{ct} value increased to 0.33 kohm, which is attributed to the presence of SnO_2 nanoparticles onto Au electrode and reduced the transfer ability of the electrons at the electrode-electrolyte solution interface. After the ethephon adsorption, R_{ct} continuously increased to 0.66 kohm. It is mainly due to the coverage of ethephon on the surface which subsequently inhibits electron access to the modified surface and further leads to the low electron transfer efficiency of the system. As for the EIS measurements of the ethephon adsorption on the surface of PANI and SnO_2@PANI nanocomposites, the similar trends of the continuous increase of R_{ct} during the procedure of the ethephon detection were observed (Fig. 4c and d).

The efficiency of ethephon detection based on the different sensors was also evaluated. Differences in the R_{ct} values before and after the generation of a new adhesive layer (ΔR_{ct}) could represent its relative amount [43]. The simulated values of R_{ct} for each stage in ethephon detection for the three samples are shown in Fig. 4d. Among the three samples, the addition of nanomaterials, i.e., PANI, SnO_2, and SnO_2@PANI, onto the Au electrode led to the variation in R_{ct}, ΔR_{ct} = 0.5, 0.21, and 1.61 kohm, respectively. After ethephon detection, substantial differences were observed among the ΔR_{ct} values for the composite electrode modified by PANI, SnO_2, and SnO_2@PANI sensor. Among the three electrochemical sensors based on the pristine SnO_2 nanoparticles, PANI, and PANI@SnO_2 nanocomposite, PANI@SnO_2-based sensor showed the best affinity for ethephon and resulted in the highest variation in R_{ct} =

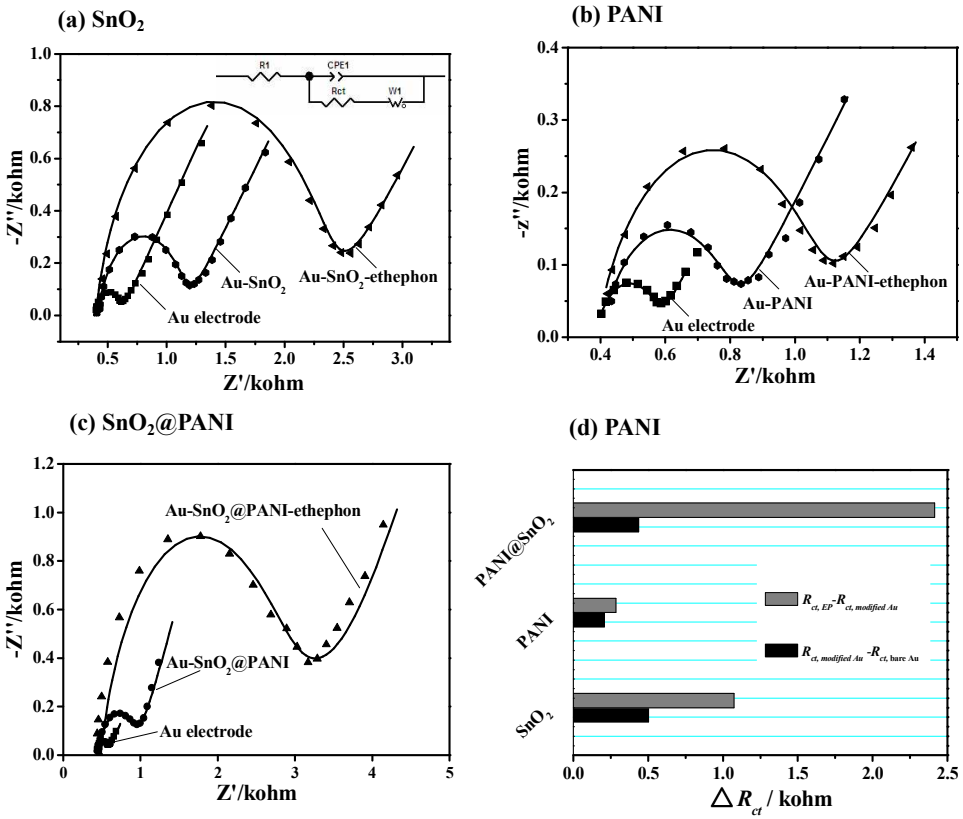

Fig. 4 EIS spectra during ethephon detection based on the electrosensor of (a) SnO_2, (b) PANI, and (c) SnO_2@PANI and the difference of R_{ct} during Au electrode modification and ethephon detection.

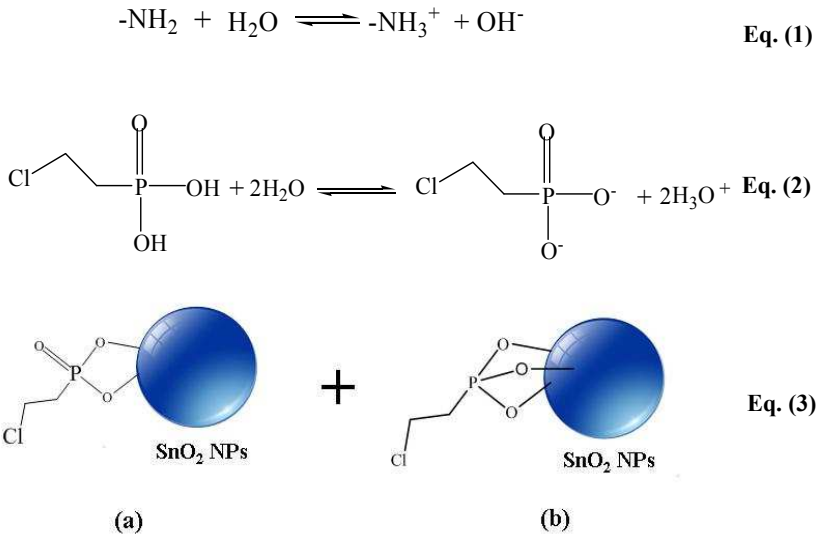

Scheme 1 Eq. (1-2) Equations of ammonium cation formation in SnO_2@PANI and phosphate anion in ethephon and Eq. (3) Schematic of ethephon adsorption onto the SnO_2 NP surface.

2.17 kohm, whereas only ΔR_{ct} = 0.29 kohm was calculated in the based system was in the intermediate between PANI and SnO_2@PANI samples, resulting in ΔR_{ct} = 1.1 kohm after ethephon detection. Evidently, the synergistic effect between PANI and SnO_2 for ethephon adsorption could be produced, leading to the detection of more ethephon molecules.

Mechanism of ethephon adsorption onto SnO_2@PANI surface

The acting force for the adsorption of the small molecules onto the nanomaterial surface mainly includes covalent bonding, electrostatic interaction, and van der Waals force. Among these forces, covalent bonding is the strongest interaction, resulting in close adhesion of small molecules onto the material surface. Ethephon detection based on the developed electrochemical biosensor of SnO_2@PANI nanocomposites is attributed to the synergistic effect between PANI and SnO_2 nanomaterials. As shown in Eq. (1) (Scheme 1), large amounts of amino groups in the PANI molecular chains are present and ionized to ammonium cations in the aqueous solution. On the contrary, the phosphate groups in ethephon are ionized to phosphate anions [Eq. (2) in Scheme 1]. Consequently, strong electrostatic interaction between the ammonium cations and the phosphate anions could take place, leading to adsorption of ethephon on the PANI nanomaterial surface. Meanwhile, ethephon could also be adsorbed onto the SnO_2 NP surface through two kinds of interaction (Eq. (3) a and b in Scheme 1) [49], in which the chemical bond of Sn-O is formed between the phosphate groups and SnO_2 [50]. For the adsorption of ethephon onto the surface of SnO_2@PANI nanocomposite, the synergy effects of PANI and SnO_2 toward ethephon adsorption could take place, resulting in more ethephon binding. Another influencing factor that should be considered is the larger specific area of the nancomposite of SnO_2@PANI compared with the individual nanomaterial [51].

The detection limitation of the developed ethephon sensor

The limit of detection (LOD), defined as the lowest concentration at which the analytical process can reliably differentiate from

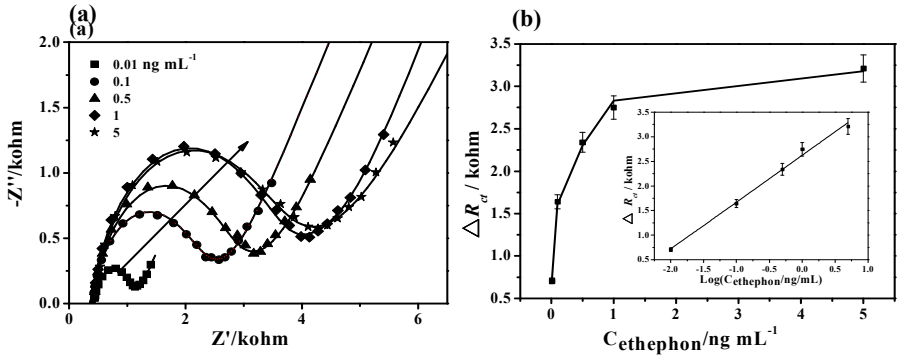

Fig. 5 (a) Nyquist diagrams recorded using the Au electrode modified by the SnO_2@PANI nanofilm adsorbed with ethephon at different concentrations: 0.01, 0.1, 0.5, 1, and 5 ng mL^{-1} and (b) Linear calibration curve for the ΔR_{ct} value versus log$C_{ethephon}$.

background levels, was accepted when the intensity of the signal is three times the background noise. To estimate the efficiency of ethephon detection, the Nyquist plots of SnO_2@PANI-modified Au electrodes adsorbed with different concentrations of ethephon within the range from 0.01 to 5 ng mL^{-1} are shown in Fig. 5a. With the increase in ethephon concentration, the R_{ct} value increased corresponding with the formation of its adsorption onto the composite surface. The difference between the R_{ct} values of the composite electrode before and after the ethephon adsorption, $\triangle R_{ct} = R_{ct,ethepon} - R_{ct,composite\ electrode}$, was adopted as the measurement signal. Herein, Freundlich adsorption equations are frequently employed to describe the adsorption process.

Freundlich adsorption equation:

$$\triangle R_{ct} = a + b \log C_e, \quad \textit{Eq.} \ (4)$$

where C_e is the concentration of ethephon (ng mL^{-1}), $\triangle R_{ct}$ is the adsorption capacity (kohm). *a* and *b* are the constants [52]. It shows the $\triangle R_{ct}$ value was linear with the logarithm of ethephon concentration (Fig. 5b). The dynamic detection range for SnO_2@PANI nanomaterial was from 0.01 to 5 ng mL^{-1}, with regression equation $\triangle R_{ct} = 2.63 + 0.95 \log_{Cethephon}$ (R^2=0.992). The LOD (S/N = 3) was 4.76 pg mL^{-1}. In addition, the analytical performance of the developed sensor for ethephon detection was compared with those of other assay methods reported in the literature, which are summarized in Table 1. The linear range and LOD of the proposed sensor significantly improved, and a lower LOD was also achieved.

Interference study

The interfering signal caused by the most common pesticides was investigated. The signal of a 3 ng mL^{-1} ethephon was compared with the signal obtained in the presence of the interfering species. The interfering study results were summarized in Fig. 6. The experiment results demonstrated that no substantial changes in ΔR_{ct} response were determined in the presence of the 3 ng mL^{-1} common peptides, such as glyphosate, direct subsidy, cholothalonil, bordeaux mixture, and marathon, at the same operating potential in the system. However, some pesticides such as Hg^{2+}, methyl parathion, carbofuran, and p-nitrophenol somehow interfered with the detection (Fig. S3).

Table 1 Assay techniques for ethephon detection

Detection technology	Detection Range/Concentration Levels	LOD	Ref.
Gas chromatograph/mass spectrometry	10-1000 ng mL^{-1}	0.004 ng	1
Ion-pairing liquid chromatography combined with tandem mass spectrometry (triple quadrupole)	0.05 mg kg^{-1}	0.02 mg kg^{-1}	7
Inductively coupled plasma mass spectrometry	10 - 25 ng mL^{-1}	1.4 ng mL^{-1}	10
Gas chromatography with cubic mass spectrometry	0.1-1.0 ng mL^{-1}	0.1 ng mL^{-1}	53
Chromatography tandem mass spectrometry	0.050-0.200 mg kg^{-1}	0.025 mg kg^{-1}	54

Repeatability, reproducibility and stability studies

The chemical stability of the resultant electrochemical sensor ensures that the sensor can be regenerated under proper conditions. In this study, the sensor was regenerated with 0.1 M HCl solution because of the disruption of the disassociation of ethephon and SnO_2@PANI nanocomposites. The sensor was first challenged with 0.1 ng mL^{-1} ethephon solution to obtain a response signal, followed by rinsing with 0.1 M HCl solution. Afterward, signal of the blank solution was recorded again. The above procedure was repeated continuously for 10 times (Fig. 7). The results suggest that the response signal to the same concentration of ethephon only attenuates by approximately 7.3% after 10 cycles, indicating the fine regeneration ability of the developed ethephon sensor.

Analysis of real samples

To evaluate the accuracy of an analytical approach, spike recovery is a useful tool. Table 2 showed the results obtained by analysis of these spike samples. The recoveries of orange juice, apple juice, strawberry juice, and lake water samples were

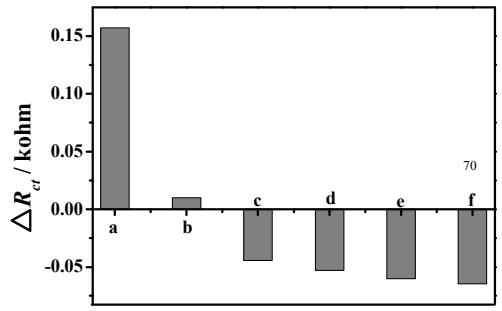

Fig. 6 ΔR_{ct} values for the ethephon detection in the presence of 3 ng mL^{-1} (a) ethephon, (b) glyphosate, (c) direct subsidy, (d) cholothalonil, (e) bordeaux mixture, and (f) marathon.

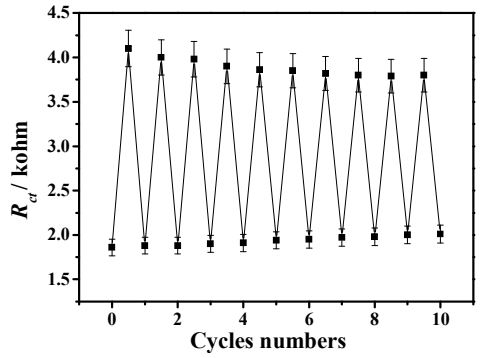

Fig. 7 Reusability of the SnO_2@PANI-based ethephon sensor challenged with 0.1 ng mL^{-1} ethephon and washed with 0.1 M HCl solution.

Table 2 Recovery studies of spiked practical samples by EIS (n=5)

Sample	Added (ng mL^{-1})	Found (ng mL^{-1})	Recovery (%)	RSD
Orange juice	0.00	Not detected	-	-
	0.10	0.096	96.0	4.3
	1.00	0.982	98.2	3.9
	5.00	4.920	98.4	3.8
Apple juice	0.00	Not detected	-	-
	0.10	0.107	107.0	4.7
	1.00	0.978	97.8	4.1
	5.00	5.120	102.4	3.7
Strawberry	0.00	Not detected	-	-
juice	0.10	0.095	95.0	4.5
	1.00	1.070	107.0	4.9
	5.00	4.750	95.0	5.8
lake water	0.00	Not detected	-	-
	0.10	0.106	106.0	4.8
	1.00	1.050	105.0	4.6
	5.00	4.950	99.0	3.2

observed in the range of 95.0%-107.0%, indicating low matrix effect on the R_{ct} response. A recovery close to 100% was expected is there were no interferences or matrix effect. The low relative standard deviations for orange and apple demonstrated the high precision of the developed electrochemical biosensor based on SnO_2@PANI nanocomposites.

Conclusions

A novel SnO_2@PANI composite was used as an efficient ethephon detection platform to develop a highly sensitive EIS ethephon sensor. Compared with individual PANI- or SnO_2-modified electrodes, the results demonstrated that the synergistic effect of the SnO_2@PANI composite could efficiently increase the electrochemical signal and be used as a classic sensor for ethephon detection. The LOD of ethephon was evaluated by the titration of ethephon concentration and measured by EIS, providing low value of 4.76 pg mL^{-1} within the range of 0.01 to 5 ng mL^{-1}. The constructed biosensor also exhibited many advantages such as good fabrication reproducibility, acceptable stability, fast response and low limit detect. This result also suggests that this simple and feasible method could be used as a sensitive layer for the detection of other food additives.

Acknowledgements

This work was supported by Program for the National Natural Science Foundation of China (NSFC: Account No. 51173172 and 21104070) and Science and Technology Opening Cooperation Project of Henan Province (Account No. 132106000076).

Notes and references

1 S. Takenaka, *J. Agr. Food Chem.* 2002, **50**, 7515-7519.
2 C. A. Kan, and J. C. Jonker-Den Rooyen, *J. Agr. Food Chem.* 1978, **26**, 470-472.
3 N. Zhang, and J. E.Casida, *Bioorg. Med. Chem.* 2002, **10**, 1281-1290.
4 J. E. Haux, G. B. Quistad, and J. E. Casida, *Chem. res. toxicol.* 2000, **13**, 646-651.
5 G. Cho, D. Kim, H. Pedersen, and C. K. Chin, *Biotechnol. progr.* 1988, **4**, 184-188.
6 L. Van Loon, and J. Antoniw, *Netherlands Journal of Plant Pathology* 1982, **88**, 237-256.
7 J. M. Marín, Ó. J. Pozo, J. Beltrán, and F. Hernández, *Rapid commun. mass sp.* 2006, **20**, 419-426.
8 J. f. Kuang, Y. Zhang, J. Chen, Q. Chen, Y. Jiang, H. Lin, S. Xu, and W. Lu, *Gene* 2011, **485**, 1-6.
9 M. S. Liyasova, L. M. Schopfer, S. Kodani, S. R. Lantz, J. E. Casida, and O. Lockridge, *Chem. res. toxicol.* 2013, **26**, 422-431.
10 Z. X. Guo, Q. Cai, and Z. Yang, *Rapid commun. mass sp.* 2007, **21**, 1606-1612.
11 C. Huybrechts, T. Deckers, and R. Valcke, *International Conference: Postharvest Unlimited* 2002, **599**, 243-247.
12 J. Lei, and H. Ju, *Chem. Soc. Rev.* 2012, **41**, 2122-2134.
13 D. Kato, N. Sekioka, A. Ueda, R. Kurita, S. Hirono, K. Suzuki, and O. Niwa, *Angew. Chem.* 2008, **120**, 6783-6786.
14 H. Dong, J. Lei, L. Ding, Y. Wen, H. Ju, and X. Zhang, *Chem. rev.* 2013, **113**, 6207-6233.
15 M. Nanu, J. Schoonman, and A. Goossens, *Adv. Mater.* 2004, **16** , 453-456.
16 Z. Zhang, H. Song, S. Zhang, J. Zhang, W. Bao, Q. Zhao, and X. Wu, *Cryst. Eng. Comm.* 2014, **16**, 110-115.
17 M. K. Patel, J. Singh, M. K. Singh, V. V. Agrawal, S. Ansari, and B. Malhotra, *J. nanosci. nanotechno.* 2013, **13**, 1671-1678.
18 Y. Wang, H. D. Tran, L. Liao, X. Duan, and R. B. Kaner, *J.Am. Chem. Soc.* 2010, **132**, 10365-10373.
19 Y. Liao, C. Zhang, Y. Zhang, V. Strong, J. Tang, X. G. Li, K. Kalantar-Zadeh, E. M. Hoek, K. L. Wang, and R. B. Kaner, *Nano lett.* 2011, **11**, 954-959.
20 Y. Ishiguro, S. Inagi, and T. Fuchigami, *Langmuir* 2011, **27**, 7158-7162.
21 R. S. Saberi, S. Shahrokhian, and G. Marrazza, *Electroanalysis* 2013, **25**, 1373-1380.
22 S. Sarmah, and A. Kumar, *B. Mater. Sci.* 2013, **36**, 31-36.
23 G. Khuspe, S. Navale, D. Bandgar, R. Sakhare, M. Chougule, and V. Patil, *Electron. Mater. Lett.* 2014, **10**, 191-197.
24 L. Wang, L. Chen, B. Yan, C. Wang, F. Zhu, X. Jiang, Y. Chao, and G. Yang, *J. Mater. Chem. A* 2014, **2**, 8334-8341.
25 Y. Jin, and M. Jia, *Colloid. Surface. A* 2015, **464**, 17-25.
26 X. Shen, L. Ma, M. Gan, Z. Li, J. Yan, S. Xie, H. Yin, and J. Zhang, *Synthetic Met.* 2014, **196** (2014) 20-26.
27 Z. A. Hu, Y. L. Xie, Y. X. Wang, L. P. Mo, Y. Y. Yang, and Z. Y. Zhang, *Mater. Chem. Phys.* 2009, **114**, 990-995.
28 A. Sadek, W. Wlodarski, K. Shin, R. B. Kaner, and K. Kalantar-Zadeh, *Nanotechnology* 2006, **17**, 4488.
29 K. R. Brown, A. P. Fox, and M. J. Natan, *J. Am. Chem. Soc.* 1996, **118**, 1154-1157.

30 J. Zhang, S. Wang, M. Xu, Y. Wang, H. Xia, S. Zhang, X. Guo and S. Wu, *J. Phys. Chem. C* 2009, **113**, 1662-1665.
31 H. M. Xiong, D. P. Liu, H. Zhang, and J. S. Chen, *J. Mater. Chem.* 2004, **14**, 2775-2780.
32 B. L. Cushing, V. L. Kolesnichenko, and C. J. O'Connor, *Chem. Rev.* 2004, **104**, 3893-3946.
33 K. Nejati, *Crystal Research and Technology*, 2012, **47**, 567-572.
34 L.G. Gai, G.J. Du, Z.Y. Zuo, Y.M. Wang, D. Liu and H. Liu, *J. Phys. Chem. C* 2009, **113**,7610-7615.
35 L.X. Zhang, P. Liu and Z. X. Su, *Polym. Degrad. Stab.* 2006, **91**, 2213-2219.
36 Y. Qiu and L. Gao, *J. Phys. Chem. B* 2005, **109**,19732-19740
37 H. Y Xua, X. Q Chen, J. Zhang, J. Q Wang, B. Q Cao and D. L. Cui, *Sensor. Actuat. B: Chem.* 2013, **176**, 166-173.
38 H. Liu, X. B. Hu, J. Y. Wang and R.I. Boughton, *Macromolecules* 2002, **35**, 9414-9419.
39 Z. H. Zhang, C. L. Feng, *Appl. Surf. Sci.* 2007, **253**, 8915–8922.
40 Y. Chen, R. Haddon, S. Fang, A. Rao, P. Eklund, W. Lee, E. Dickey, E. Grulke, J. Pendergrass and A. Chavan, *J. Mater. Res.*, 1998, **13**, 2423-2431.
41 W. L. Zhang, B. J. Park and H. J. Choi, *Chem. Commun.*, 2010, 46, 5596-5598.
42 L. S. Zhang, L. Y. Jiang, H. J. Yan, W. D. Wang, W. Wang, W. G. Song, Y. G. Guo and L. J. Wan, *J. Mater. Chem.*, 2010, **20**, 5462-5467.
43 A. Li, F. Yang, Y. Ma and X. R. Yang, *Biosen. Bioelectron.* 22 (2007) 1716.
44 J. Yue and A. Epstein, *Macromolecules*, 1991, **24**, 4441-4445.
45 K. Ghanbari, S. Bathaie and M. Mousavi, *Biosen. Bioelectron.*, 2008, **23**, 1825-1831.
46 A. Bogomolova, E. Komarova, K. Reber, T. Gerasimov, O. Yavuz, S. Bhatt and M. Aldissi, *Anal. Chem..*, 2009, **81**, 3944-3949.
47 I. O. K'Owino and O. A. Sadik, *Electroanal.*, 2005, **17**, 2101-2113
48 Z. Zhang, S. Liu, Y. Shi, Y. Zhang, D. Peacock, F. Yan, P. Wang, L. He, X. Feng and S. Fang, *J. Mater. Chem. B*, 2014, **2**, 1530-1538
49 R. F. de Castilho, E. B. R. de Souza, R. V. da Silva Alfaya, and A. A. da Silva Alfaya, *Electroanal.* 2008, **20**, 157-162.
50 L. Kőrösi, S. Papp, V. Meynen, P. Cool, E. F. Vansant, and I. Dékány, *Colloid. Surf.* 2005, **268**, 147-154.
51 Z. Zhang, L. Luo, H. Chen, M. Zhang, X. Yang, S. Yao, J. Li, and M. Peng, *Electroanal.*, 2011, **23**, 2446-2455.
52. J A. X. Li, F. Yang, Y. Ma and X. R. Yang, *Biosen. Bioelectron.* 2007, **22**, 1716.
53 A. Royer, F. Laporte, S. Bouchonnet, and P. Y. Communal, *J. Chromatogr. A* 2006, **1108**, 129-135.
54 V. Hanot, L. Joly, A. Bonnechère, and J. Van Loco, *Food Anal. Methods* 2015, **8**, 524-530.

Graphical Abstract

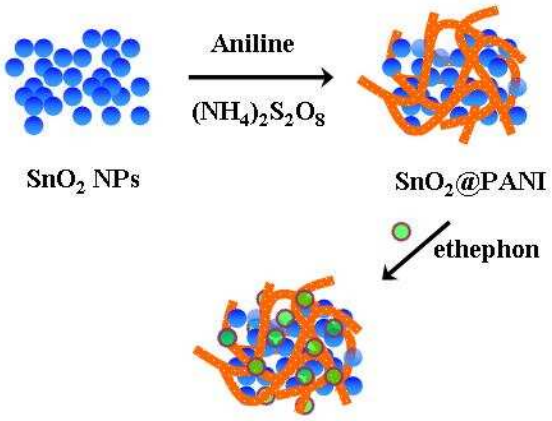

The nanocomposites from polyaniline and stannic oxide (SnO_2@PANI) were synthesized and developed as electrode materials for ethephon detection. The developed SnO_2@PANI nanocomposite possesses good electrochemical performance with relatively low charge-transfer resistance. It exhibits good selectivity and stability. All of these food performances provide a promising tool to detect the illegal food additives.